Molecular Crystals and Liquid Crystals

ISSN: 1542-1406 (Print) 1563-5287 (Online) Journal homepage: http://www.tandfonline.com/loi/gmcl20

# Characteristics of $Cu_2ZnSn(S_{1-x}Se_x)_4$ Thin Films Crystallized with Various Sulfur and Selenium Vapor Sources

Chan Kim & Sungwook Hong

**To cite this article:** Chan Kim & Sungwook Hong (2015) Characteristics of $Cu_2ZnSn(S_{1-x}Se_x)_4$ Thin Films Crystallized with Various Sulfur and Selenium Vapor Sources, Molecular Crystals and Liquid Crystals, 617:1, 195-203, DOI: 10.1080/15421406.2015.1076327

**To link to this article:** http://dx.doi.org/10.1080/15421406.2015.1076327

*Mol. Cryst. Liq. Cryst.*, Vol. 617: pp. 195–203, 2015

ISSN: 1542-1406 print/1563-5287 online
DOI: 10.1080/15421406.2015.1076327



# Characteristics of $Cu_2ZnSn(S_{1-x}Se_x)_4$ Thin Films Crystallized with Various Sulfur and Selenium Vapor Sources

CHAN KIM[1] AND SUNGWOOK HONG[2,*]

[1]Department of Physics, Kyungpook National University, Daegu, Korea
[2]Division of Science Education, Daegu University, Gyeongsan, Korea

*$Cu_2ZnSn(S_{1-x}Se_x)_4$ photoabsorbers were fabricated by annealing multi layered metal precursors with sulfur and selenium powders in evacuated and sealed quartz ampules. The Se composition x in the $Cu_2ZnSn(S_{1-x}Se_x)_4$ thin films was controlled by varying the ratio of the powders in the ampules. As x was changed, the diffraction angles 2θ of the main peaks of the $Cu_2ZnSn(S_{1-x}Se_x)_4$ crystals varied between 28.42° for x = 0 and 27.07° for x = 1. Similarly, the lattice constants a and c increased from 0.54293 and 1.08573 nm for x = 0 to 0.57002 and 1.13754 nm for x = 1, respectively, with nearly zero deviation parameter. The band gap energy decreased with increasing x, from 1.403 eV for x = 0 to 0.836 eV for x = 1, and the band gap bowing parameter was 0.028 eV.*

**Keywords** CZTS; $Cu_2ZnSnS_4$; CZTSSe; Solar cell; Band gap energy; Photovoltaics; bowing parameter; Vegard's law

## Introduction

Earth-abundant copper–zinc–tin–chalcogenide kesterites, $Cu_2ZnSnS_4$ (CZTS) and $Cu_2ZnSnSe_4$ (CZTSe), have attracted increasing attention in the last few years for use as photoabsorbers in solar cell devices [1–3]. $Cu_2ZnSnS_4$ and $Cu_2ZnSnSe_4$ are known to have the properties of p-type semiconductors with theoretical direct band gap energies of 1.5 and 0.96 eV, respectively, and an absorption coefficient of $10^4$ $cm^{-1}$ in the visible light range [1, 4]. The experimental band gap energies of these photoabsorbers are reportedly around 1.5 eV for CZTS and around 0.8 eV for CZTSe [2, 5]. Moreover, the direct band gap energy of $Cu_2ZnSn(S,Se)_4$ (CZTSSe) ranges from 1.0 to 1.5 eV [6–8]. Thus, CZT-based chalcopyrite-type photoabsorbers are promising candidates for next-generation thin-film solar cells. The best photovoltaic conversion efficiency of 12.6% has been reported for CZTSSe-based solar cell device fabricated by hydrazine solution process [9]. Although the hydrazine solution process yielded a device with the highest conversion efficiency, this process has problems such as undesired impurities and chemical toxicity. Thus, solar cell devices fabricated using vacuum processes have the potential to realize higher energy conversion efficiencies. CZT-based absorbers with the highest reported energy conversion

*Address correspondence to Prof. Sungwook Hong, Division of Science Education, Daegu University, Jillyang, Gyeongsan, Gyeongbuk 712-714, Korea (ROK). E-mail: swhong@daegu.ac.kr

Color versions of one or more of the figures in the article can be found online at www.tandfonline.com/gmcl.

efficiencies have band gap energies between 1.05 and 1.2 eV [9–11]. The optimized band gap energy of the solar cell was theoretically reported to be 1.4 eV [12]. To improve the energy conversion efficiency of CZT-based solar cell devices, a method of tuning the energy band gap of the photoabsorber is required. To date, CZT-based solar cells have been fabricated by vacuum processes using metal precursors having a stacked structure [13] that are partially deposited [14] or co-deposited [15–16] from each elemental source. The surface morphology of the metal precursor is reportedly an important parameter for improving the conversion efficiency of a solar cell [1], and a Zn layer coupled with a Cu–Sn co-sputtered layer has yielded a very good surface morphology [17].

In this study, six layers of metal precursors, each consisting of a coupled Zn/Cu–Sn layer, were deposited using RF–magnetron sputtering equipment. CZTSSe photoabsorbers were crystallized in evacuated and sealed quartz ampules at an annealing temperature of 550°C and the molar ratio was controlled by varying the amount of S and Se powder. We investigated the effect of the Se composition of the CZTSSe crystal on the interplanar spacing $d$ of the crystal, lattice constants $a$ and $c$ of the tetragonal structure, and band gap energy and band gap bowing parameter according to Vegard's law.



## Experimental

CZT-based photoabsorbers were fabricated by an annealing process using multilayered metal precursors. Metal precursor layers were grown on soda-lime glass by RF magnetron sputtering with single sources of Cu, Zn, and Sn targets. Each metal precursor layer consisted of a coupled Zn and Cu–Sn layer co-sputtered with Cu and Sn single targets. Because the co-sputtered Cu and Sn layer has a good surface morphology [17], a Cu and Sn layer was co-sputtered at an RF power of 100 W for 5 min. A Zn layer was then sputtered at an RF power of 110 W for 5 min. This deposition process was repeated six times. The measured thickness of the multilayered metal precursor was about 600 nm. The background pressure of the deposition chamber was less than $1.5 \times 10^{-6}$ Torr. The metal precursor was deposited under an Ar gas pressure of 5.5 mTorr and an Ar gas flow rate of 10 sccm.

$Cu_2ZnSn(S_{1-x}Se_x)_4$ thin films were crystallized by an annealing process in evacuated and sealed ampules with S and Se vapor partial pressures determined by the molar ratio of the two powders. The quartz ampules had an internal volume of about 15 $cm^3$. When the Se mole fraction of the powder in the ampules was increased from $x = 0$ to $x = 1$ in steps of 0.02 mmol, the S mole ratio was decreased from $1 - x = 1$ to $1 - x = 0$. The total amount of sulfur and selenium powder used was fixed at 0.01 mmol. Table 1 lists the contents and mole ratios of S and Se in the ampules. The ampules containing the sulfur and selenium powders and the metal precursors (12.5 cm × 25.0 cm) were annealed at 550°C in a quartz furnace for 10 min with insertion and release times of 10 s. Once released, the ampules were

**Table 1.** Ratios of S to Se in the powder in evacuated ampules before annealing and in the CZTSSe crystal in the absorber after annealing, as determined using EDX

| | | #1 | #2 | #3 | #4 | #5 | #6 | #7 |
|---|---|---|---|---|---|---|---|---|
| S:Se ratio | powder | 1.0:0.0 | 0.8:0.2 | 0.6:0.4 | 0.5:0.5 | 0.4:0.6 | 0.2:0.8 | 0.0:1.0 |
| | CZTSSe | 1.00:0.00 | 0.94:0.06 | 0.86:0.14 | 0.83:0.17 | 0.75:0.25 | 0.57:0.43 | 0.00:1.00 |

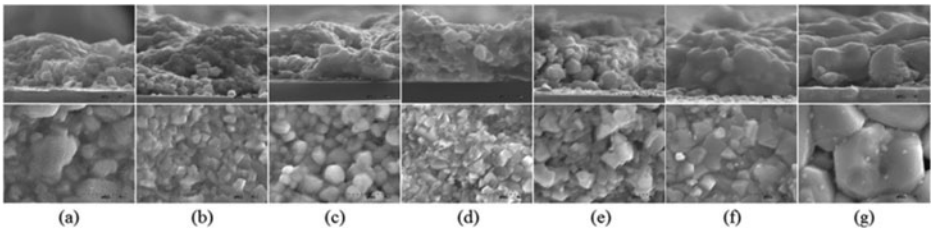


**Figure 1.** SEM images of the surface morphology and cross section of $Cu_2ZnSn(S_{1-x}Se_x)_4$ films formed by sulfo-selenization of six Zn/Cu–Sn layers on soda-lime glass: (a) $Cu_2ZnSnS_4$, (b) $Cu_2ZnSn(S_{0.94}Se_{0.06})_4$, (c) $Cu_2ZnSn(S_{0.86}Se_{0.14})_4$, (d) $Cu_2ZnSn(S_{0.83}Se_{0.17})_4$, (e) $Cu_2ZnSn(S_{0.75}Se_{0.25})_4$, (f) $Cu_2ZnSn(S_{0.57}Se_{0.43})_4$, (g) $Cu_2ZnSnSe_4$.



allowed to cool naturally for 30 min on an aluminum sheet at room temperature. After the cooling process, sulfur and selenium remained on the inner walls of the ampules that were in contact with the aluminum sheet. This meant that an excess of either sulfur or selenium was supplied for CZTSSe crystallization in the ampules.

The surface morphology, thickness, and chemical composition of the thin films were analyzed by field-emission scanning electron microscopy (FE-SEM, Hitachi S-4300) and energy-dispersive X-ray spectroscopy (EDX, Horiba EDX system). The crystalline and optical properties of the thin films were analyzed by X-ray diffraction (XRD, PANalytical X'pert Pro-MPD goniometer) and UV-vis-NIR spectrometry (Carry 5000), respectively.

## Results and Discussion

Table 1 lists the molar ratios of S and Se powders in the ampule before annealing and in the $Cu_2ZnSn(S_{1-x}Se_x)_4$ crystal after annealing. The molar ratio of S and Se in the CZTSSe crystal after annealing differs from that of the powders in the ampules before annealing. Although the amount of Se in samples #5 and #6 was higher than the amount of S before annealing, the corresponding CZTSSe crystals contained less Se than S after annealing. This result can be explained as follows: S, with a melting point of 119.0°C at 1 atm, melted and diffused into the metal precursor before Se, with a melting point of 221°C at 1 atm, did during annealing in the evacuated ampules. Thus, Se either diffused to vacancies or was replaced by S in the CZTS crystal.

As shown in Fig. 1, the $Cu_2ZnSn(S_{1-x}Se_x)_4$ grains were smaller than the CZTS and CZTSe crystals. This result confirms that there are more crystal seeds, which determined the grain size of the crystal, in CZTSSe than in CZTS ($x = 0$) and CZTSe ($x = 1$). The $Cu_2ZnSn(S_{1-x}Se_x)_4$ thin films were around 2 $\mu$m thick, as shown in Fig. 1. Table 2 lists the chemical composition ratios of the CZTSSe thin films as determined using EDX. The elemental composition was obtained by averaging five points with square areas of 10 $\mu$m $\times$ 10 $\mu$m in the SEM images. All the samples had a high Cu content and low S and Se contents. The compositional ratios of Zn and Sn matched the stoichiometry of CZTSSe well.

Figure 2 shows the XRD patterns of the CZTSSe thin films. The (112) main peaks of $Cu_2ZnSnS_4$ and $Cu_2ZnSnSe_4$ clearly appeared at 28.42° and 27.07°, respectively [18–19]. The (220) and (132) peaks, which had the second- and the third-highest relative intensities, respectively, are also prominent. When the Se composition $x$, defined by the ratio Se/(S + Se), was increased, the peaks in the XRD patterns were shifted leftward. The reason is that

**Table 2.** Chemical composition ratios of CZTSSe thin films determined using EDX

| | Cu/(Zn+Sn) | Zn/Sn | Metal/(S + Se) |
|---|---|---|---|
| $Cu_2ZnSnS_4$ | 1.24 | 0.96 | 1.25 |
| $Cu_2ZnSn(S_{0.94}Se_{0.06})_4$ | 1.15 | 1.00 | 1.20 |
| $Cu_2ZnSn(S_{0.86}Se_{0.14})_4$ | 1.13 | 1.01 | 1.23 |
| $Cu_2ZnSn(S_{0.83}Se_{0.17})_4$ | 1.20 | 0.95 | 1.26 |
| $Cu_2ZnSn(S_{0.75}Se_{0.25})_4$ | 1.18 | 0.85 | 1.23 |
| $Cu_2ZnSn(S_{0.57}Se_{0.43})_4$ | 1.14 | 0.95 | 1.28 |
| $Cu_2ZnSnSe_4$ | 1.26 | 0.84 | 1.29 |



as the $x$ was increased, S, which has an atomic size of 1.84 Å, was replaced by Se, which has an atomic size of 1.98 Å. Thus, the interplanar spacing d increases, and the diffraction angle $2\theta$ decreases. The relative intensity of the CZTSe (x = 1) crystal was higher than that of the other crystals under the same XRD measurement conditions. This result shows that CZTSe was better crystalized than the other compounds at the same annealing temperature and pressure. The shift in the (112) peaks is shown as an inset in Fig. 2.

Figure 3 shows the $2\theta$ values of the (112) main peaks and the interplanar spacing $d$ of the CZTSSe crystals as a function of the selenium composition $x$. When $x$ was increased, the $2\theta$ value of the (112) main peaks decreased linearly, whereas the interplanar spacing d increased linearly. We found that the interplanar spacing d increased proportionally from 3.1404 Å for $x = 0$ to 3.2929 Å for $x = 1$. This result shows that CZTSSe could be crystallized in the same structure as the CZTS and CZTSe host crystals over the entire

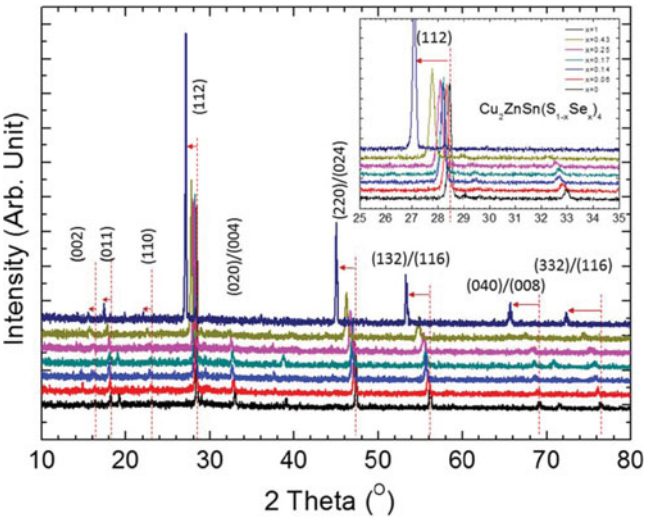


**Figure 2.** XRD patterns of CZTSSe absorbers formed by sulfo-selenization of multistacked precursors with various Se compositions $x$ between 0 and 1 after annealing at 550°C. Inset shows magnification of the shift in the (112) main peaks of the absorbers.

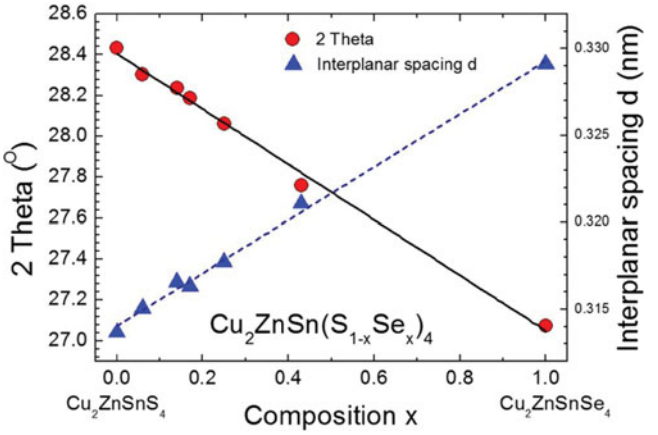


**Figure 3.** Diffraction angle $2\theta$ and interplanar spacing $d$ for the (112) main peaks in CZTSSe films as a function of Se composition $x$, defined as the ratio Se/(S + Se).

compositional range without phase transformation, in accordance with Vegard's law [15, 20–21].

Figure 4 shows the full width at half-maximum (FWHM) of the three main peaks, (112), (024), and (132), in the XRD patterns of the CZTSSe crystals as a function of the Se composition $x$. When $x$ was increased, the FWHMs of these peaks increased, with the exception of the peaks of the CZTSe crystal ($x = 1$). This result corroborates the result of the SEM analysis (Fig. 1) that the grain sizes of CZTS for $x = 0$ and of CZTSe for $x = 1$ are larger than that of the CZTSSe crystal. The FWHMs of the host crystals CZTS and CZTSe were less than those of CZTSSe. This result shows that internal stress exists in the CZTSSe crystal.

CZTS and CZTSe crystals have a tetragonal structure, namely, the kesterite or stannite structure [22]. CZTSSe also crystallizes in a tetragonal structure. The lattice constants of

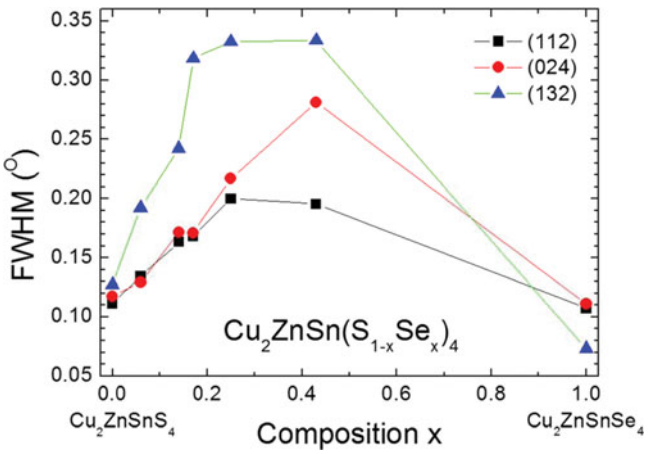


**Figure 4.** FWHM of XRD main peaks, (112), (024), and (132), for CZTSSe films as a function of Se composition $x$.

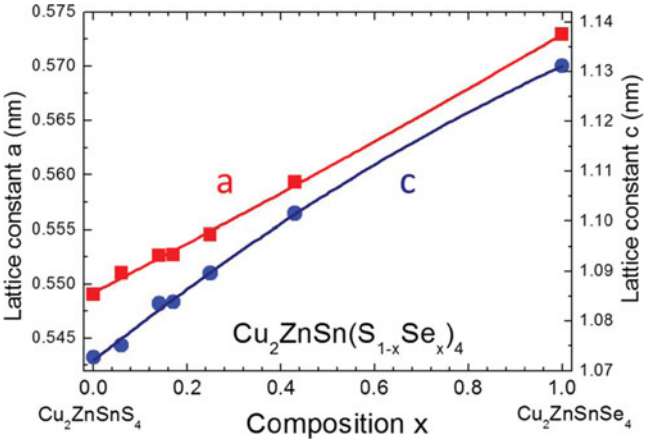


**Figure 5.** Lattice constants of CZTSSe thin films, which follow Vegard's law with deviation parameters of $\delta_a = -0.0073$ nm and $\delta_c = 0.00339$ nm, which are close to zero.

the tetragonal structure can be obtained from the XRD patterns as follows:

$$\frac{4\sin^2\theta}{\lambda^2} = \frac{h^2 + k^2}{a^2} + \frac{l^2}{c^2}$$

where $h$, $k$, and $l$ are the Miller indices of the plane. Figure 5 shows the lattice parameters of the CZTSSe thin films obtained from the (220), (132), and (040) XRD peaks. The variation in the lattice constants as a function of the Se composition $x$ was in good agreement with Vegard's law [23], which is expressed as

$$\mathrm{a}\,(\mathrm{x}) = x a_{CZTSe} + (1 - \mathrm{x})\, a_{CZTS} - \delta_a x\,(1 - x)$$

Here, $a(x)$ is the lattice constant of the $Cu_2ZnSn(S_{1-x}Se_x)_4$ crystal, whereas, $a_{CZTS}$ and $a_{CZTSe}$ are those of the $Cu_2ZnSnS_4$ and $Cu_2ZnSnSe_4$ crystals, respectively. Furthermore, the lattice constant $c$ can be expressed in the same manner as the lattice constant $a$. The deviation parameter for the lattice constants $a$ or $c$ is $\delta$. According to Vegard's law, the lattice constants of an alloy consisting of two materials that have a cubic structure change linearly as a function of the molar ratio x of the substitutional material. However, the change in the lattice constants of the $Cu_2ZnSn(S_{1-x}Se_x)_4$ crystal with a tetragonal structure is not exactly linear with variation in the Se composition $x$. The degree of deviation from this linearity is called the deviation parameter $\delta$. According to the result of the data fitting in Fig. 5, the lattice constants $a$ and $c$ of CZTS were determined to be 0.54293 and 1.08573 nm, respectively, and those of CZTSe were determined to be 0.57002 and 1.13754 nm, respectively. The deviation parameters of $a$ and $c$, $\delta_a$ and $\delta_c$, were determined to be $-0.0073$ and 0.00339 nm, respectively. This result reflects the fact that the lattice constants $a$ and $c$ of $Cu_2ZnSn(S_{1-x}Se_x)_4$ vary almost linearly with $x$ from the lattice constants of $Cu_2ZnSnS_4$ to those of $Cu_2ZnSnSe_4$, because $\delta$ is close to zero.

The absorption coefficient $\alpha$ was determined from the transmittance of the CZTSSe thin films using a UV-vis-NIR spectrometer. The relationship between the absorption coefficient $\alpha$ and band gap energy $E_g$ of a semiconductor is expressed as [24]

$$\alpha = \mathrm{A}(h\nu - E_g)^n / h\nu$$

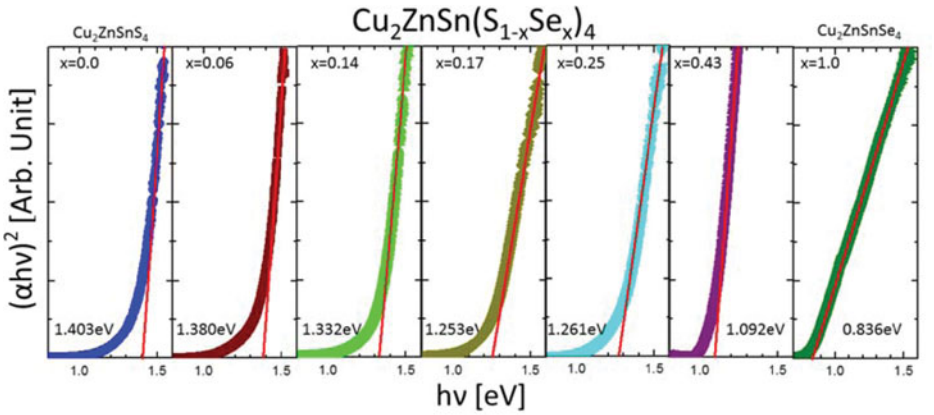


**Figure 6.** Plot of $(\alpha h\nu)^2$ versus the photon energy $h\nu$ for $Cu_2ZnSn(S_{1-x}Se_x)_4$ thin films.

where $A$ is a constant, $h$ is the Planck's constant, and $\nu$ is the frequency of the photons. The constant $n$ is 1/2 for a direct transition and 2 for an indirect transition [24]. Figure 6 shows $(\alpha h\nu)^2$ versus the photon energy $h\nu$ for the CZTSSe thin films. The band gap energy of the CZTSSe thin films, which was determined by extrapolating the straight line fit of the $(\alpha h\nu)^2$ versus $h\nu$ curve to the intercept on the photon energy axis, ranged from 1.203 eV for CZTS to 0.836 eV for CZTSe.

Figure 7 shows the band gap energy of the CZTSSe thin films as a function of the Se composition x. As for the lattice constants, Vegard's law for band gap energy is expressed as

$$E_g(x) = xE_{g,CZTS} + (1 - x)E_{g,CZTSe} - x(1 - x)E_b$$

where $E_b$ is called the band gap bowing parameter and represents the deviation from linearity of the energy band gap change with changes in $x$. The best fit to the results in

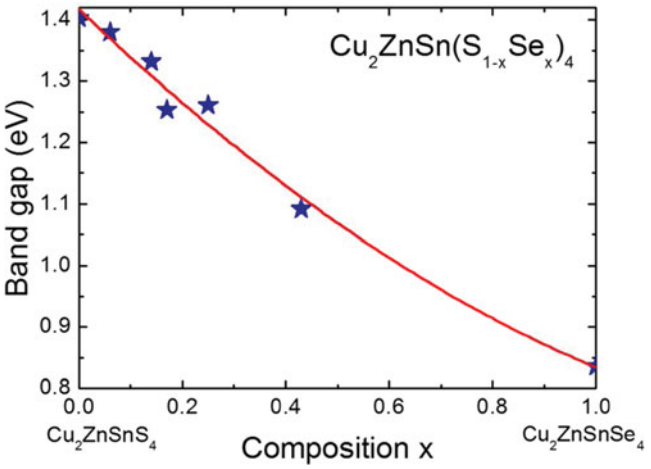


**Figure 7.** Band gap energy of the $Cu_2ZnSn(S_{1-x}Se_x)_4$ thin film as a function of Se composition $x$, which follows Vegard's law with a band gap bowing parameter of 0.228 eV.

Fig. 7 using Vegard's law yields a band gap bowing parameter of 0.028 eV. The band gap energy of the films varied by as $x$ was changed from 0 to 1. These results should be useful for improving the photovoltaic energy conversion efficiency.

## Conclusions

$Cu_2ZnSn(S_{1-x}Se_x)_4$ photoabsorber layers were fabricated by annealing a multilayered Zn/Cu–Sn metal precursor with sulfur and selenium powders in evacuated and sealed ampules. The molar ratio of Se in the CZTSSe crystals was controlled by varying the molar ratio of the S and Se powders in the ampules. The molar ratio of S and Se in the CZTSSe crystals differed from that of the S and Se powders in the ampules. As the Se composition $x$ was increased, the diffraction angles $2\theta$ of the XRD pattern decreased, and the interplanar spacing $d$ of the CZTSSe crystals increased. The composition dependence of the lattice constants $a$ and $c$ was in good agreement with Vegard's law with nearly zero deviation. The lattice constants $a$ and $c$ varied from 0.54293 and 1.08573 nm for $x = 0$ to 0.57002 and 1.13754 nm for $x = 1$, respectively. The energy band gap decreased as a function of $x$ from 1.403 eV for $x = 0$ to 0.836 eV for $x = 1$, and the band gap bowing parameter was 0.028 eV. The results of this study can contribute to the fabrication of solar cells having better photovoltaic efficiency with a tunable band gap energy.

## Funding

This study was supported by the Daegu University Research Grant, 2014.

## References

[1] Katagiri, H. (2005). *Thin Solid Films*, 480–481, 426.
[2] Zoppi, G., Forbes, I., Miles, R. W., Dale, P. J., Scragg, J. J., & Peter, L. M. (2009). *Prog. Photovoltaics*, *17*, 315.
[3] Mitzi, D. B., Gunawan, O., Todorov, T. K., Wang, K., & Guha, S. (2011). *Sol. Energy Mater. Sol. Cells*, *95*, 1421.
[4] Friedlmeier, T. M., Wieser, N., Walter, T., Dittrich, H., & Schock, H. W. (1997). *Proceedings of the 14th European Photovoltaic Specialists Conference, Barcelona*, 1242.
[5] Kim, C., & Hong, S. (2013). *Mol. Cryst. Liq. Cryst.*, *586*, 147.
[6] Ito, K., & Nakazawa, T. (1998). *Jpn. J. Appl. Phys.*, *27*, 2094.
[7] Rajeshmon, V. G., Kartha, C. S., Vijayakumar, K. P., Sanjeeviraja, C., Abe, T., & Kashiwaba, Y. (2011). *Solar Energy*, *85*, 249.
[8] Matsushita, H., Maeda, T., Katsui, A., & Rakizawa, T. (2000). *J. Cryst. Growth*, *208*, 416.
[9] Wang, W., Winkler, M. T., Gunawan, O., Gokmen, T., Todorov, T. K., Zhu, Y., & Mitzi, D. B. (2013). *Adv. Energy Mater*, http://dx.doi.org/10.1002/aenm.201301465.
[10] Todorov, T. K., Reuter, K. B., & Mitzi, D. B. (2010). *Adv. Mater. 22*, E156.
[11] Guo, Q., Ford, G. M., Yang, W., Walker, B. C., & Stach, E. A. (2010). *J. Am. Chem. Soc. 132*, 17384.
[12] Niki, S., Contreras, M., Repins, I., Powalla, M., Kushiya, K., Ishizuka, S. & Matsubara, K. (2010). *Prog. Photovolt: Res. Appl.*, *18*, 453.
[13] Araki, H., Mikaduki, A., Kubo, Y., Sata, T., Jimbo, K., Maw, W.S., Katagiri, H., Yamazaki, M., Oishi, K., & Takeuchi, A. (2008). *Thin Solid Films*, *517*, 1457.
[14] Kim, C., Hong, S., Bae, H., Rhee, I., Kim, H. T., Kim, D., & Kang, J. (2013). *Mol. Cryst. Liq. Cryst.*, *586*, 154.
[15] Momose, N., Htay, M. T., Sakurai, K., Iwano, S., Hashimoto, Y., & Ito, K. (2012). *Appl. Phys. Express*, *5*, 081201.

[16] Redinger, A., & Siebentritt, S. (2012). *Appl. Phys. Lett.*, *97*, 092111.
[17] Hong, S. (2012). *Mol. Cryst. Liq. Cryst.*, *565*, 153.
[18] Menchetti, S., Bernardini, G.P., Bindi, L., & Bonazzi, P. (2003). *Canadian Mineralogist*, *41*, 639.
[19] Marchuk, O. V., Parasyuk, O. V., Piskach, L. V., Dydchak, I. V., Gulay, L. D., & Olekseyuk, I. D. (2002). *Journal of Alloys Compd.*, *340*, 141.
[20] Denton, A. R., & Ashcroft, N. W. (1991). *Phys. Rev. A 43*, 3161.
[21] Riha, S. C., Parkinson, B. A., & Prieto, A. L. (2011). *J. Am. Chem. Soc.*, *133*, 15272.
[22] Chen, S. Gong, X. G., Walsh, A., & Wei, S. (2009). *Appl. Phys. Lett. 94*, 041903.
[23] Kuo, Y., Liou, B., Yen, S., & Chu, H. (2004). *Optics Communication 237*, 363.
[24] Pawar, S. M., Moholkar, A. V., Rajpure, K. Y., & Bhosal, C. H. (2006). *J. Phys. Chem. Solids 67*, 2386.